













# The bursty origin of the Milky Way thick disc

Sijie Yu <sup>1</sup>★, James S. Bullock <sup>1</sup>, Courtney Klein <sup>1</sup>, Jonathan Stern <sup>2,3</sup>, Andrew Wetzel <sup>4</sup>,  
Xiangcheng Ma <sup>5</sup>, Jorge Moreno <sup>6</sup>, Zachary Hafen <sup>1</sup>, Alexander B. Gurvich <sup>2</sup>, Philip F. Hopkins <sup>7</sup>,  
Dušan Kereš<sup>8</sup>, Claude-André Faucher-Giguère <sup>2</sup>, Robert Feldmann <sup>9</sup> and Eliot Quataert<sup>10</sup>

<sup>1</sup>Department of Physics and Astronomy, University of California Irvine, Irvine, CA 92697, USA

<sup>2</sup>Department of Physics & Astronomy and CIERA, Northwestern University, 1800 Sherman Ave, Evanston, IL 60201, USA

<sup>3</sup>School of Physics & Astronomy, Tel Aviv University, Tel Aviv 69978, Israel

<sup>4</sup>Department of Physics and Astronomy, University of California, Davis, CA 95616, USA

<sup>5</sup>Department of Astronomy and Theoretical Astrophysics Center, University of California Berkeley, Berkeley, CA 94720, USA

<sup>6</sup>Department of Physics and Astronomy, Pomona College, Claremont, CA 95616, USA

<sup>7</sup>TAPIR, Mailcode 350-17, California Institute of Technology, Pasadena, CA 91125, USA

<sup>8</sup>Department of Physics and Center for Astrophysics and Space Science, University of California at San Diego, 9500 Gilman Drive, La Jolla, CA 92093, USA

<sup>9</sup>Institute for Computational Science, University of Zurich, Zurich CH-8067, Switzerland

<sup>10</sup>Department of Astrophysical Sciences, Princeton University, Princeton, NJ 08544, USA

Accepted 2021 May 4. Received 2021 April 22; in original form 2021 March 5

## ABSTRACT

We investigate thin and thick stellar disc formation in Milky Way-mass galaxies using 12 FIRE-2 cosmological zoom-in simulations. All simulated galaxies experience an early period of bursty star formation that transitions to a late-time steady phase of near-constant star formation. Stars formed during the late-time steady phase have more circular orbits and thin-disc-like morphology at  $z = 0$ , while stars born during the bursty phase have more radial orbits and thick-disc structure. The median age of thick-disc stars at  $z = 0$  correlates strongly with this transition time. We also find that galaxies with an earlier transition from bursty to steady star formation have a higher thin-disc fractions at  $z = 0$ . Three of our systems have minor mergers with Large Magellanic Cloud-size satellites during the thin-disc phase. These mergers trigger short starbursts but do not destroy the thin disc nor alter broad trends between the star formation transition time and thin/thick-disc properties. If our simulations are representative of the Universe, then stellar archaeological studies of the Milky Way (or M31) provide a window into past star formation modes in the Galaxy. Current age estimates of the Galactic thick disc would suggest that the Milky Way transitioned from bursty to steady phase  $\sim 6.5$  Gyr ago; prior to that time the Milky Way likely lacked a recognizable thin disc.

**Key words:** methods: numerical – Galaxy: disc – galaxies: formation – galaxies: evolution – galaxies: star formation.

## 1 INTRODUCTION

Milky Way-mass disc galaxies in the local Universe, including our own, are often characterized by a thin-disc component embedded within a thicker disc, which accounts for  $\sim 10$ – $15$  per cent of total disc luminosity (van der Kruit & Freeman 2011). The Milky Way itself has a distribution of disc stars that can be decomposed into thin and thick components spatially (Gilmore & Reid 1983; Jurić et al. 2008; Bensby et al. 2011; Bovy & Rix 2013). Thicker-disc stars tend to be older, more metal poor, and more  $\alpha$ -enhanced (Fuhrmann 1998; Prochaska et al. 2000; Bensby et al. 2005; Lee et al. 2011; Haywood et al. 2013; Recio-Blanco et al. 2014; Hayden et al. 2015; Hayden et al. 2017; Mackereth et al. 2017; Sharma et al. 2019). These characteristics may be loosely interpreted as evidence that thick-disc stars formed early and rapidly, perhaps in a series of bursts (e.g. van der Kruit & Freeman 2011). Snaith et al. (2014) use elemental abundances of long-lived stars to derive a star formation history a Milky Way thick-disc population and conclude that these stars emerged during an early, elevated period of star formation,

and that the Galactic thick disc may be comparable *in mass* (not luminosity) to the young ( $< 8$  Gyr old) thin disc.

While it is natural to think of the thin/thick-disc dichotomy as reflecting the existence of two distinct and separate kinematic populations, the Milky Way appears to have a continuous distribution of disc thicknesses that vary smoothly with fixed abundance (Bovy, Rix & Hogg 2012). There is certainly a dichotomy in the ratio of  $\alpha$  to iron (at low iron) in the solar vicinity, though the relative distributions of high and low  $\alpha$  elements vary smoothly with location in the disk (e.g. Hayden et al. 2015; Weinberg et al. 2019). These trends may be explained without requiring a distinct thick-disc component that emerged from a separate evolutionary path (e.g. Sharma, Hayden & Bland-Hawthorn 2020). Nevertheless, it is useful to use the terms ‘thick disc’ and ‘thin disc’ as a shorthand classification to help us compare and contrast stars with more eccentric orbits that take them farther from the disc plane to those with more circular orbits that align tightly within it.

Despite years of study, an understanding of how thick and thin populations arise within the broader story of galaxy formation remains a key question. One of the most enduring ideas is that pre-existing thin discs are heated in mergers with small satellite galaxies to create a vertically extended component (Quinn, Hernquist &

\* E-mail: [sijiey3@uci.edu](mailto:sijiey3@uci.edu)

Fullagar 1993; Kazantzidis et al. 2008; Purcell, Kazantzidis & Bullock 2009). In fact, the phase-space structure of stars in the solar neighbourhood provides some evidence that such an event – the Gaia-Enceladus Sausage merger – may have been significant enough to heat a proto Milky Way disc, under the assumption that a thin disc existed at this early time (Belokurov et al. 2018; Helmi et al. 2018).

However, the chemical abundance structure of the Milky Way disfavors the idea that thick-disc formation is associated with a single discrete event (Freudenburg et al. 2017). Rather, these data favour an ‘upside down’ formation scenario – first predicted by cosmological simulations (Brook et al. 2004, 2006, 2012; Bird et al. 2013) – where stars are born in relatively thick discs at early times, and only later form in thin discs.

Many recent cosmological simulations naturally produce  $z = 0$  discs with young stars concentrated in a thinner component than old stars (e.g. Ma et al. 2017b; Grand et al. 2018; Navarro et al. 2018; Pillepich et al. 2019; Park et al. 2020; Bird et al. 2021). These same simulations at high redshift produce discs that are systematically thicker and clumpier than those at low redshift, as observed in nearly all deep, high-resolution imaging studies of galaxies (Elmegreen & Elmegreen 2006; Elmegreen et al. 2007; Genzel et al. 2008; Shapiro et al. 2008; Overzier et al. 2010; Elmegreen et al. 2017). The observed transition from thick irregular galaxies at high redshift to thin rotation-dominated discs at low redshift is well established, and often referred to as ‘disc settling’ (Kassin et al. 2012).

Whilst upside-down disc formation is seen regularly in simulations, the physical origin of this thick-to-thin transition has been hard to distill. One idea is that discs are born thick during an early period of gas-rich mergers (Brook et al. 2004). At high redshift, high star formation rate (SFR) densities, high gas fractions, and feedback-induced turbulence can also contribute to an initially hot disc (Lehnert et al. 2014). An alternative possibility is that stars are initially born in thin discs, but are quickly and continuously heated owing to chaotic accretion of gas (Meng & Gnedin 2021). In some simulations, most stars are born kinematically hotter at early times and subsequently heated after birth on a short time-scale (Ma et al. 2017b; Bird et al. 2021).

In this paper, we explore the transition from thick- to thin-disc formation in 12 Milky Way-mass galaxies drawn from FIRE-2 cosmological zoom-in simulations. As seen in previous work (Brook et al. 2004; Bird et al. 2013; Ma et al. 2017b; Navarro et al. 2018; Park et al. 2020; Bird et al. 2021), our discs tend to form upside down, with the thick discs in place early and the thin disc forming at late times. One new finding in our work is that the transition from thick to thin-disc formation correlates with a transition in star formation mode, from an early, elevated bursty phase with highly time-variable SFR, to a late-time steady phase of near-constant SFR. Thin-disc stars tend to be born during the late-time steady phase, whilst thick-disc stars are associated with the latter part of the bursty phase. Galaxies with older thick-disc populations have an earlier transition from bursty to steady star formation. The earlier the transition time, the more dominant the thin disc is at  $z = 0$ .

A transition from bursty to steady star formation has been reported previously in the FIRE simulations, at  $z = 0.5$ – $1.5$  in Milky Way-mass haloes (Muratov et al. 2015; Anglés-Alcázar et al. 2017a, b; Sparre et al. 2017; Faucher-Giguère 2018). In particular, Stern et al. (2020) show that the transition to steady star formation coincides with the virialization of the inner circumgalactic medium (CGM). Specifically, when haloes in FIRE cross a characteristic mass scale ( $\sim 10^{12} M_{\odot}$ ), the cooling time of shocked gas in the inner halo ( $0.1 R_{\text{vir}}$ ) exceeds the local free-fall time. This creates a hot confining medium, with high and nearly uniform thermal pressure. After this time, Stern et al. (2020) observes that star formation becomes less

bursty and gaseous discs become more rotationally supported. This steady, settled disc phase may be enabled by the hot, pressurized inner CGM itself, which may prevent supernova-driven outflows from repeatedly blowing out the interstellar medium (ISM) in a way that would otherwise might perturb disc structure (e.g. Martizzi 2020).

Of particular relevance is work by Ma et al. (2017b), who used a slightly lower resolution FIRE-1 zoom-in simulation to show that disc stars at large scale height (thick-disc stars) form primarily during an early chaotic bursty mode, whilst younger stars were formed in a more stable disc. In what follows, we perform a more systematic analysis using a larger, higher resolution sample of FIRE-2 haloes and confirm that this result is more general. This motivates us to suggest that the physical transition from bursty to steady star formation also coincides with a shift from thick-disc to thin-disc formation in Milky Way-mass galaxies. If this is true in the real Universe, then stellar archaeological studies of the Milky Way could provide a window into past star formation modes, as well as the build-up of the Galactic CGM.

The outline of this manuscript is as follows. In Section 2, we provide an overview of our simulations and present our kinematic definition of thin- and thick-disc stars. Section 3 presents results focusing for two illustrative cases (Section 3.1) and then on to explore general trends for all galaxies in our sample (Section 3.3). We conclude and discuss our results in the context of the Milky Way in Section 4.

## 2 SIMULATIONS AND METHODS

### 2.1 FIRE-2 simulations of Milky Way-mass galaxies

Our analysis utilizes cosmological zoom-in simulations performed with the multimethod gravity plus hydrodynamics code GIZMO (Hopkins 2015) from the Feedback In Realistic Environments (FIRE) project.<sup>1</sup> We rely on the FIRE-2 feedback implementation (Hopkins et al. 2018) and the mesh-free Lagrangian Godunov (MFM) method. The MFM approach provides adaptive spatial resolution and maintains conservation of mass, energy, and momentum. FIRE-2 includes radiative heating and cooling for gas across a temperature range of  $10$ – $10^{10}$  K. Heating sources include an ionizing background (Faucher-Giguère et al. 2009), stellar feedback from OB stars, AGB mass-loss, type Ia and type II supernovae, photoelectric heating, and radiation pressure – with inputs taken directly from stellar evolution models. The simulations self-consistently generate and track 11 elemental abundances (H, He, C, N, O, Ne, Mg, Si, S, Ca, and Fe), and include sub-grid diffusion of these elements in gas via turbulence (Hopkins 2016; Su et al. 2017; Escala et al. 2018). Star formation occurs in gas that is locally self-gravitating, sufficiently dense ( $> 1000 \text{ cm}^{-3}$ ), Jeans unstable and molecular (following Krumholz & Gnedin 2011). Locally, star formation efficiency is set to 100 per cent per free-fall time, i.e.  $\text{SFR}_{\text{particle}} = m_{\text{particle}} \times f_{\text{mol}} / t_{\text{ff}}$ , where  $f_{\text{mol}}$  is the self-shielded molecular fraction of each gas particle and  $t_{\text{ff}}$  is the free-fall time. Gas particles are converted to stars at this rate stochastically (Katz, Weinberg & Hernquist 1996). Note that this does *not* imply that the global efficiency of star formation is 100 per cent within a giant-molecular cloud (or across larger scales). Self-regulated feedback limits star formation to  $\sim 1$ – $10$  per cent per free-fall time (Faucher-Giguère et al. 2009; Hopkins 2017; Orr et al. 2018).

In this work, we analyse 12 Milky Way-mass galaxies (Table 1). These zoom simulations are initialized following Oñorbe et al. (2014). Six of these galaxies (with names following the convention

<sup>1</sup><https://fire.northwestern.edu/>

**Table 1.** The simulations we employ in this work. We list the following: the name of the zoom-in target halo, the stellar mass ( $M_*$ ) within the central 20 kpc of the halo at  $z = 0$ , the radius ( $R_{90}$ ) enclosing 90 per cent of  $M_*$ , the halo virial mass ( $M_{\text{halo}}$ ), the halo virial radius ( $R_{\text{halo}}$ ), the resolution of each simulation quantified by the initial baryonic particle mass ( $m_i$ ), and the reference that first introduced each halo at the quoted targeted resolution. The remaining columns present derived quantities: the lookback time to the end of the bursty phase/onset of the steady phase ( $t_B$ ), the mass-weighted thin-disc fraction ( $f_{\text{thin disc m}}$ ), the luminosity-weighted thin-disc fraction ( $f_{\text{thin disc l}}$ ), the median thick-disc age ( $t_{50}$ ), and the 90 per cent oldest star of the thick disc ( $t_{90}$ ). Hosts with names starting with ‘m12’ are isolated configurations selected from the Latte suite, whilst the rest are in LG-like pairs from the ELVIS on FIRE suite. The four galaxies marked with an asterisk correspond to short-lived, late-time bursts of star formation taking place after the onset of the steady phase. Three of these four bursts appear to be triggered by minor mergers. The exception is *Thelma*, which has late-time star formation in the ‘steady’ regime (by our formal definition), but is still experiencing fairly variable star formation compared to most of our galaxies at late times. These bursts and/or mergers tend to influence  $t_{90}$  but do not significantly affect  $t_{50}$  nor  $f_{\text{thin disc}}$ . The haloes are ordered by decreasing  $t_B$ , from  $t_B = 6.52$  Gyr (Romeo, top) to  $t_B = 0.0$  Gyr (m12w, bottom).

Simulation name	$M_*$ ( $M_\odot$ )	$R_{90}$ (kpc)	$M_{\text{halo}}$ ( $M_\odot$ )	$R_{\text{halo}}$ (kpc)	$m_i$ ( $M_\odot$ )	$t_B$ (Gyr)	$f_{\text{thin disc m}}$ ( $M$ weighted)	$f_{\text{thin disc l}}$ ( $L$ weighted)	Thick disc $t_{50}$ (Gyr)	Thick disc $t_{90}$ (Gyr)	Reference
Romeo	$7.4 \times 10^{10}$	13.3	$1.0 \times 10^{12}$	317	3500	6.52	0.45	0.70	8.96	6.16	A
m12b*	$8.1 \times 10^{10}$	9.8	$1.1 \times 10^{12}$	335	7070	6.32	0.37	0.64	7.34	2.72	A
Remus	$5.1 \times 10^{10}$	12.3	$9.7 \times 10^{11}$	320	4000	5.88	0.36	0.62	8.22	4.88	B
Louise	$2.9 \times 10^{10}$	12.0	$8.5 \times 10^{11}$	310	4000	5.56	0.32	0.65	8.11	4.06	A
m12f*	$8.6 \times 10^{10}$	11.0	$1.3 \times 10^{12}$	355	7070	5.01	0.38	0.65	6.28	2.62	C
Romulus	$1.0 \times 10^{11}$	14.2	$1.5 \times 10^{12}$	375	4000	4.90	0.37	0.69	7.37	4.92	B
Juliet	$4.2 \times 10^{10}$	9.6	$8.5 \times 10^{11}$	302	3500	4.40	0.30	0.62	6.74	4.66	A
m12m	$1.1 \times 10^{11}$	11.3	$1.2 \times 10^{12}$	342	7070	3.81	0.34	0.58	6.07	3.24	E
m12c*	$6.0 \times 10^{10}$	9.7	$1.1 \times 10^{12}$	328	7070	3.70	0.32	0.62	5.39	2.30	A
m12i	$6.4 \times 10^{10}$	9.2	$9.0 \times 10^{11}$	314	7070	3.14	0.32	0.59	6.18	3.50	D
Thelma*	$7.9 \times 10^{10}$	12.4	$1.1 \times 10^{12}$	332	4000	2.57	0.27	0.57	4.73	1.95	A
m12w	$5.8 \times 10^{10}$	8.7	$8.3 \times 10^{11}$	301	7070	0.0	0.24	0.43	4.38	1.13	F

Notes. The references are: A: Garrison-Kimmel et al. (2019a), B: Garrison-Kimmel et al. (2019b), C: Garrison-Kimmel et al. (2017), D: Wetzel et al. (2016), E: Hopkins et al. (2018), F: Samuel et al. (2020).

m12\*) are isolated and part of the Latte suite (Wetzel et al. 2016; Garrison-Kimmel et al. 2017; Hopkins 2017; Garrison-Kimmel et al. 2019a). Six, with names associated with famous duos (e.g. Romeo and Juliet), are part of the ELVIS on FIRE project (Garrison-Kimmel et al. 2019a, b) and are set in Local-Group-like configurations, as in the ELVIS suite (Garrison-Kimmel et al. 2014). This suite includes three simulations, containing two MW/M31-mass galaxies each. The main haloes were selected so that they have similar relative separations and velocities as of the MW-M31 pair in the Local Group (LG). Table 1 lists the initial baryonic particle masses for each simulation. Latte gas and star particles have initial masses of  $7070 M_\odot$ , whilst ELVIS on FIRE has  $\approx 2 \times$  better mass resolution ( $m_i = 3500\text{--}4000 M_\odot$ ). Gas softening lengths are fully adaptive down to  $\approx 0.5\text{--}1$  pc. Star particle softening lengths are  $\approx 4$  pc physical and a dark matter force softening is  $\approx 40$  pc physical.

## 2.2 Defining thin and thick discs

There are multiple ways to separate a ‘thick-disc’ from a ‘thin-disc’ population in observations (Martig et al. 2016). The physical characteristics authors use to define the thick disc include geometric morphology, kinematics, chemical abundances, and age. The geometric/morphological definition is the natural choice for distant galaxies, where detailed chemical and/or age information is harder to extract.

In this theoretical analysis, we elect to define thick- and thin-disc populations using a purely kinematic definition based on each star particle’s circularity (Abadi et al. 2003), which also produces disc populations that follow the qualitative geometric expectations for thin and thick discs (see below). Whilst it is common in Milky Way studies to use elemental abundances to divide thin- and thick-disc populations, we adopt this kinematic definition in order to fully decouple our selection from the nature of star formation. Specifically, alpha enhancement correlates with starburst activity, so we would like to avoid using abundance ratios when looking for distinct correlations

related to the star formation history. The fact that we find correlations between kinetically defined thick-disc populations and the mode of star formation suggests that the correlation between thick-disc formation and star formation activity is non-trivial. Previous work by Ma et al. (2017b) find qualitatively similar results using more traditional observationally oriented definitions of the thick disc based on a vertical density profile, suggesting that the result is insensitive to the precise definition.

Our categorization is based on each star particle’s circularity,  $\epsilon = j_z/j_c(E)$ , defined as the ratio of each particle’s angular momentum to that of a circular orbit with the same energy (Abadi et al. 2003). The angular momentum direction  $\hat{z}$  is set by total stellar angular momentum within 10 kpc of each galaxy’s centre. We categorise star particles with  $\epsilon = 0.8\text{--}1$  as *thin-disc* stars, and those with  $\epsilon = 0.2\text{--}0.8$  as *thick-disc* stars. Our classification is motivated by past explorations (e.g. Abadi et al. 2003; Okamoto et al. 2010; Knebe et al. 2013), which find that the circularity correlates well with standard morphological definitions of thin- and thick-disc populations.

The left-hand and middle panels of Fig. 1 illustrate our circularity-based definitions for two specific simulations: Romeo (top) and Juliet (bottom). The left-hand panels show the mass-weighted circularity distributions and the middle panels show the luminosity-weighted circularity distributions for each galaxy. By our definitions, the magenta regions correspond to thin-disc stars, whilst the cyan regions correspond to thick-disc stars. Note that whilst the mass-weighted distributions yield approximately equal thin- and thick-disc populations, the luminosity-weighted distributions assign  $\sim 60\text{--}70$  per cent to the thin disc. The right-hand panels show luminosity-weighted images of the thin- and thick-disc populations for each galaxy, which illustrate that our orbit-based definitions yield spatial distributions that look qualitatively like discs that are indeed thin and thick.

We find that our  $\epsilon$ -based classification scheme results in thin- and thick-disc populations with vertical density profiles (in the  $z$  direction) resembling those of traditional morphologically identified



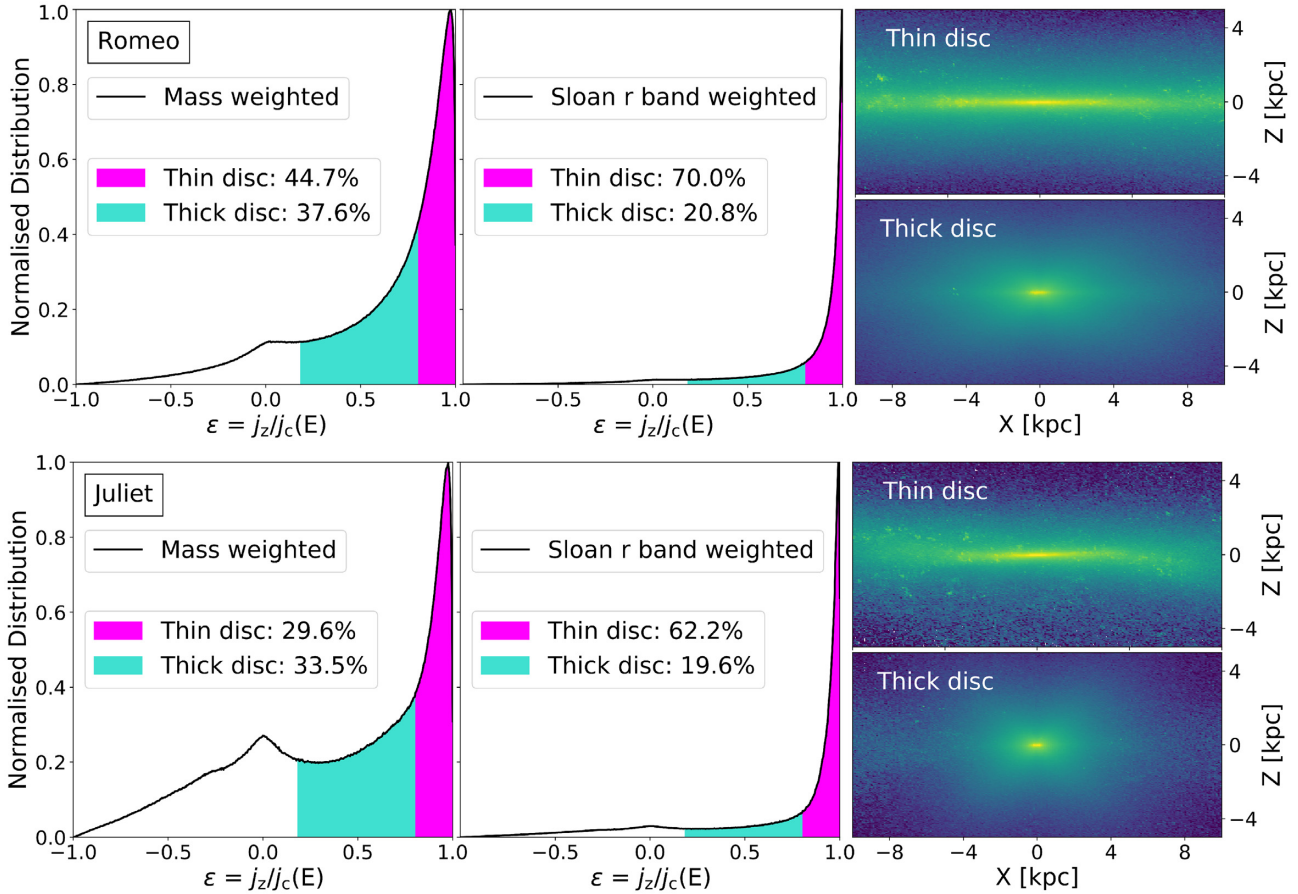


**Figure 1.** Circularity and spatial distributions of stars in Romeo (top set) and Juliet (bottom set). The *left-hand panels* show the mass-weighted distribution of circularities  $\epsilon$  of all the stars within  $R_{90}$  in the galaxies (13.3 and 9.6 kpc, respectively). See Section 2.2 for a description of  $\epsilon$ . The magenta blocks mark thin-disc stars, which we define as the stars with  $\epsilon \geq 0.8$ . The cyan blocks mark thick-disc stars, which we define to be those with  $0.8 > \epsilon \geq 0.2$ . The fraction of stars in each block is shown in the legend. The *middle panels* show the same distributions but now weighted by the Sloan  $r$ -band luminosity of each star particle. The luminosity-weighted distributions generally give a much higher thin-disc fraction. The percentages indicate mass- and luminosity-weighted fractions for each component. The *right-hand panels* display  $z = 0$  edge-on views (2D density weighted by Sloan  $r$ -band luminosity) of the thin (upper) and thick (lower) disc stars. We see that these definitions produce disc components that qualitatively resemble geometrically defined thin and thick discs.

thin and thick discs. Whilst some of our galaxies have vertical profiles better fit by exponential forms, the majority prefers  $\text{sech}^2$  fits. At mock solar locations (8 kpc from the galactic centre), fits to the resultant thin-disc populations yield scale heights for our 12 galaxies that range from  $\sim 250$  to  $\sim 800$  pc for luminosity-density profiles (in Sloan  $r$  band); and from  $\sim 500$  to  $\sim 950$  pc for mass-density profiles. Similar fits to our thick-disc populations have scale heights that range from  $\sim 1.2$  to  $1.5$  kpc for luminosity-density profiles. These results are consistent with previous analyses of FIRE simulations (e.g. Ma et al. 2017b; Sanderson et al. 2020). We find that dividing populations in this manner yields scale height results in line with those we obtain with more traditional (purely spatially based) two-component fits. We also find that our simple  $\epsilon$ -based classification yields thick-disc populations that are older, more metal poor, and more alpha enhanced than the thin discs we identify (not shown).

We note that there can be a non-trivial fraction of stars that exist at very low or negative circularities ( $\epsilon < 0.2$ ), which would naturally be associated with a spheroidal component. For example, in Fig. 1, for Romeo (Juliet), this component represents 17 per cent (37 per cent) of the mass and 6.8 per cent (13 per cent) of the light. We generally find that these spheroidal stars tend to form in the earliest periods of galaxy assembly, whilst thick-disc stars form

later. Since the focus of this paper is on thin/thick-disc formation, we have largely ignored low/negative angular momentum stars in what follows, though further investigation into the origin of the inner spheroid as it relates to star formation in the early galaxy is warranted. Such an exploration would require a more sophisticated kinematic disc/spheroidal classifications of stars with overlapping  $\epsilon$  ranges. We have performed a simple check of the sensitivity of our main results to the presence of bulge stars by neglecting all stars that sit within 1 kpc of the galactic centre of each galaxy and find that this does not change our results substantially. The fraction of stars that have  $\epsilon > 0.2$  and that sit within 1 kpc is relatively small in all of our galaxies and, when either excluded or included, have only a minor effect on the age distributions of our ‘thick-disc’ stars.

### 3 RESULTS

#### 3.1 Two illustrative cases: Romeo and Juliet

##### 3.1.1 Bursty phase, steady phase, and age distributions

The top panels in Fig. 2 show the star formation histories of Romeo (left) and Juliet (right) as a function of lookback time. The

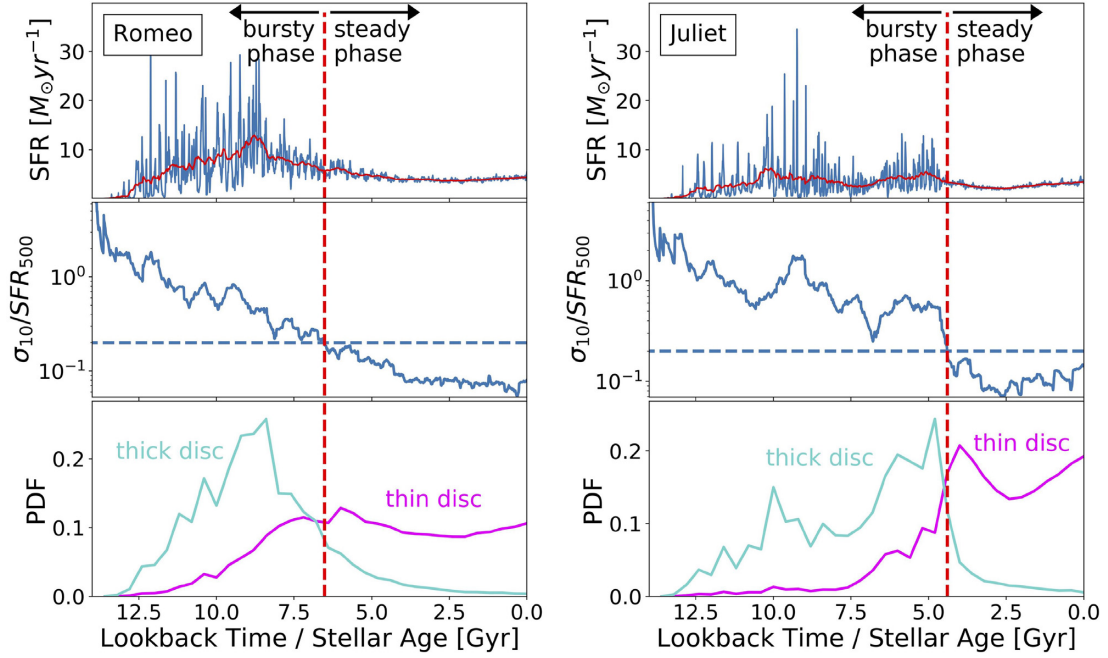


**Figure 2.** Star formation histories and thin/thick-disc stellar age distributions for Romeo (left) and Juliet (right). The *top panels* show the SFR in the galaxy as a function of lookback time. The blue lines show the ‘instantaneous’ SFR averaged over 10 Myr bins, while the red lines show the ‘smoothed’ SFR averaged over 500 Myr bins. The *middle panels* show the variance in instantaneous SFR divided by the smoothed SFR as a function of time. We see that the SFR variance in each galaxy generally decreases with time, from bursty to steady, as we approach the present day. For ease of description, we divide the star formation history of each galaxy into two distinct phases – an early bursty phase and a late steady phase – delineated a time  $t_B$  where the SFR variance falls below 0.2 times the smoothed SFR. This ‘bursty-phase lookback time’ is marked by the vertical red dashed line in each upper panel. The *bottom panels* show the age distribution of  $z = 0$  stars that belong to the thick disc (cyan) and thin disc (magenta) in each galaxy. We see that thick-disc stars have ages that track closely the bursty period of star formation while thin-disc stellar ages correspond more closely to the steady phase.

SFR<sup>2</sup> displayed is averaged over both a short time-scale of 10 Myr (SFR<sub>10</sub>, blue) and a longer time-scale of 500 Myr (SFR<sub>500</sub>, red). The middle panel shows the variance in ‘instantaneous’ SFR,  $\sigma_{10}$ , divided by the average SFR<sub>500</sub> as a function of lookback time. We define  $\sigma_{10}(t)$  as the variance in SFR<sub>10</sub> over a time range spanning  $t \pm 250$  Myr. We see that the relative variance is much larger at early times than at late times, consistent with previous studies (e.g. Stern et al. 2020; Flores Velázquez et al. 2021) that have shown that star formation in massive FIRE-2 galaxies tends to transition from bursty to steady as we approach the present day.

While the transition from bursty to steady is not always sharp, the trend is quasi-monotonic, with the ratio  $\sigma_{10}/\text{SFR}_{500}$  generally decreasing with time. For the sake of simplicity in this analysis, we find it useful to divide the star formation history of each galaxy into two distinct phases: an early bursty phase and a late-time steady phase. We define the bursty phase to end at a lookback time  $t_B$  when the variance in ‘instantaneous’ SFR first falls below  $B = 0.2$  times the time-averaged SFR:

$$\frac{\sigma_{10}(t_B)}{\text{SFR}_{500}(t_B)} \equiv B. \quad (1)$$

We use this definition to assign a specific bursty-phase time-scale to each galaxy’s star formation history. Our qualitative results are not sensitive to the precise choice of  $B = 0.2$  on the right-hand side of equation (1). Larger choices ( $B > 0.2$ ) tend to push the bursty phase slightly earlier and smaller choices ( $B < 0.2$ ) tend to push the burst

phase slightly later. By our adopted definition, Romeo has a bursty-phase lookback time of  $t_B = 6.5$  Gyr and Juliet has a bursty phase that ends more recently at  $t_B = 4.4$  Gyr. The vertical, red-dashed lines in Fig. 2 mark these times. Table 1 provides bursty-phase lookback times  $t_B$  for our simulated galaxies.

The bottom panels in Fig. 2 show the age distributions of thick-disc stars (cyan) and thin-disc stars (magenta). Thick-disc ages tend to track the bursty-phase star formation, whilst the thin-disc stars closely track the steady phase in each case. We emphasize again that in defining a specific value for  $t_B$  we do not mean to suggest that there is always a razor-sharp phase-change in star formation activity (or in disc thickness) but rather to assign a specific time-scale to each galaxy that reasonably marks a qualitative transition. We note that age-overlap of thick- and thin-disc stars in Romeo is much more significant than it is in Juliet. This mirrors the more gradual decrease in relative SFR variance in Romeo, compared to the sharp transition near  $t_B$  seen in Juliet. Nevertheless, the broad tendency for typical thick-disc stellar ages to correlate with bursty-phase lookback times is seen for every galaxy in our sample (as we show in Section 3.3).

### 3.1.2 Morphology with time

Figs 3 and 4 show images of Romeo and Juliet at three specific times in the past: 8.4, 4.7, and 2.7 Gyr ago, which also illustrate how stars that formed at these epochs are spatially distributed today. The top row (a) shows the SFR versus time. The arrow symbols on the time axis indicate the specific lookback times visualized beneath. Row (b) shows luminosity-weighted images of the main progenitor of

<sup>2</sup>These star formation histories are measured for all particles that were born within 20 kpc of the most massive progenitor.

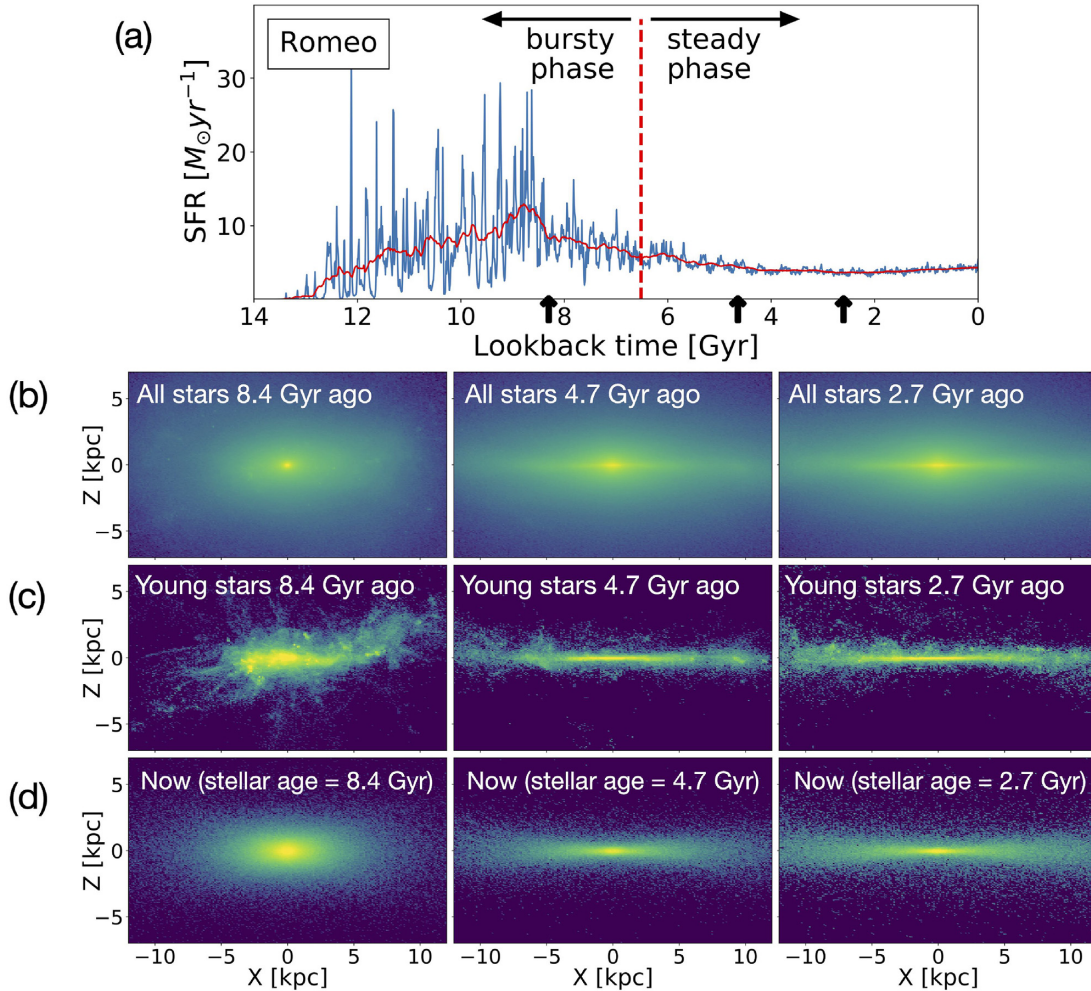


**Figure 3.** (a) Instantaneous (blue) and smoothed (red) SFR for *Romeo* plotted as a function of lookback time. The vertical red dashed line shows our adopted time that separates the bursty phase from the steady phase according to equation (1). (b) Edge-on, luminosity-weighted images for *Romeo* at three different lookback times – from left to right: 8.4, 4.7, and 2.7 Gyr. The arrows along the time axis in top panel indicate these times. (c) Edge-on, luminosity-weighted images for the youngest population (formed within 100 Myr) at the same times. (d) Edge-on, luminosity-weighted images at  $z = 0$  for the same stars shown in row c. Note that 8.4 Gyr ago, when the star formation was still bursty, the galaxy resembles a thick disc. At the later two times, in the steady phase, a thin-disc component emerges.

each galaxy at the specified times. Each snapshot is viewed edge-on with respect to the stellar angular momentum axis at that time. Row (c) includes images of the young stellar populations, corresponding to stars born within the last 100 Myr of the indicated times. Lastly, row (d) shows the current location ( $z = 0$ ) of the young stars shown in (c). Note that rows (c) and (d) are similar to fig. 1 in Ma et al. (2017b).

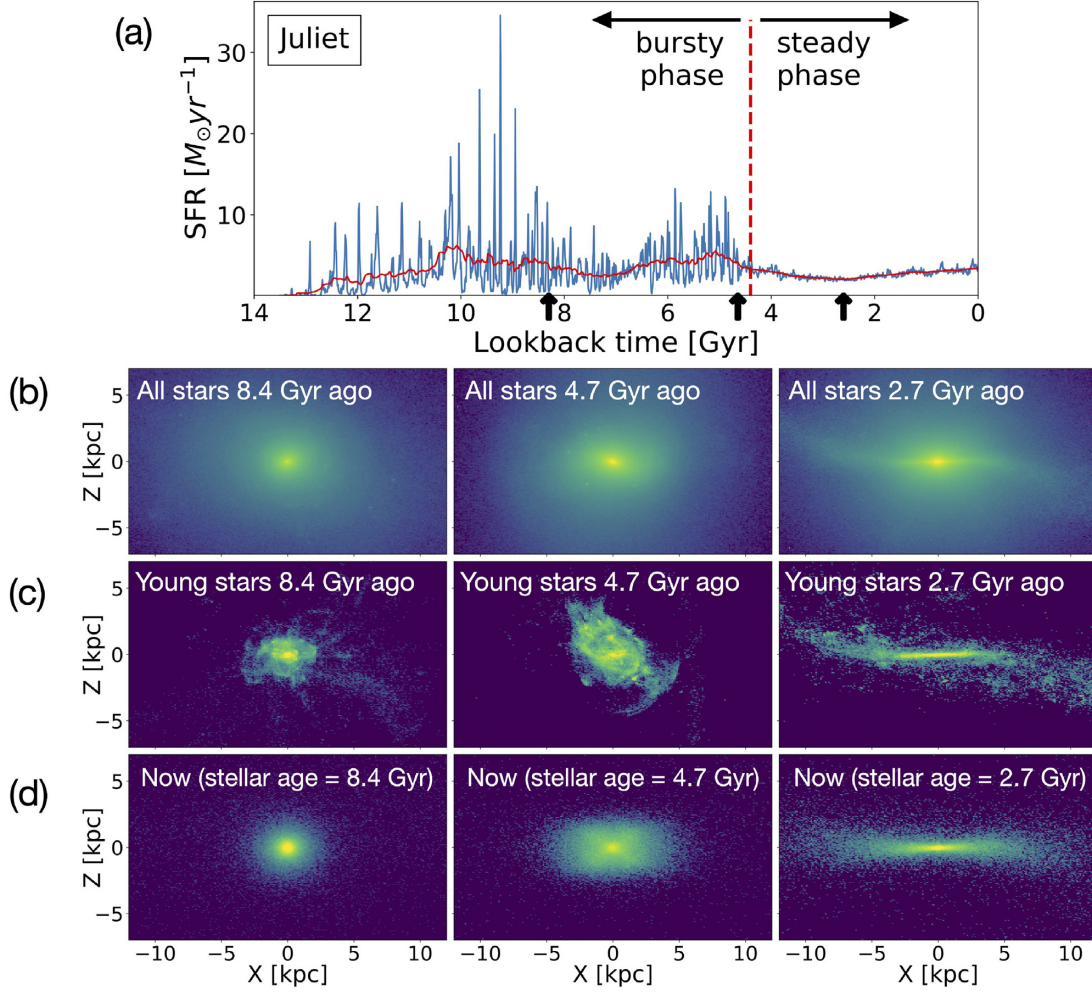
Fig. 3 shows that, 8.4 Gyr ago (prior to the end of the bursty phase) *Romeo* resembled a thick disc embedded within a significant spheroid. The stars forming at this time (panel c, far left) are not very well ordered into a thin disc, but do exhibit some coherence. Those stars today are arranged in a thick-disc like configuration (d, far left). Conversely, at 4.7 and 2.7 Gyr (after the steady phase has commenced) *Romeo*’s thin disc has fully emerged. Young stars at those times are situated in thin discs (c, middle and right) and remain in relatively thin configurations at  $z = 0$  (d, middle and right).

Fig. 4 shows that *Juliet* exhibits a transition from thick to thin, which happens later than *Romeo*’s. Concretely, whilst *Romeo* had a pronounced thin-disc component 4.7 Gyr ago, *Juliet* had no thin disc at that time. Only in the most recent image (2.7 Gyr

does *Juliet* begin to resemble a thin disc. This difference in morphological structure with time mirrors the difference we see in the transition to steady star formation. *Juliet* has a bursty phase that ends only at a lookback time of  $t_B = 4.2$  Gyr, compared to *Romeo*, which ended its bursty phase  $t_B = 6.7$  Gyr ago. At 4.2 Gyr, *Juliet* happens to have just experienced a rapid inflow of cool gas, some of which has formed stars in the thick, rotating structure we see in row (c), middle panel. Those stars end up in a thick-disc component at  $z = 0$  (row d, bottom).

The 8.4 and 4.7 Gyr panels in Fig. 4 for *Juliet* show differences in morphology with time that are representative across our larger simulated sample. Specifically, we find that the bursty phase itself can be further divided into two periods of morphological development: (1) a very early, chaotic bursty phase, where even the youngest stars ( $< 50$  Myr) have angular momenta that are misaligned with the existing stars in the galaxy; and (2) a later, quasi-stable ‘bursty-disc’ phase, where some short-lived angular momentum cohesion exists. As shown with an example in the next section, we find that stars that are born very early on, when the SFR is *very* bursty, tend to be born with spheroidal-type orbits (with peaks in the  $\epsilon$





**Figure 4.** Same as Fig. 3, now for *Juliet*. At 8.4 and 4.7 Gyr ago, when *Juliet*’s star formation was still bursty, there is no visible thin disc. Only in the 2.7 Gyr images, after the steady phase has started, is thin-disc morphology apparent.

distribution ranging from 0 to 0.3). Stars that are made during the later, quasi-stable bursty-disc phase, tend to be fairly coherent for a short period of time, with circularity distributions within  $\sim 50$  Myr of their birth that straddle thin/thick-disc characteristics (peaking with  $\epsilon \sim 0.6\text{--}0.8$ ). These bursty-disc stars are quickly heated to thicker-disc orbits within  $\sim 100$  Myr (similar to the behaviour reported by Meng & Gnedin 2021). This later heating appears to be a result of bursty feedback and chaotic accretion. Similar components could also be found based on stellar populations at  $z = 0$  using a Gaussian mixture model (Nikakhtar et al. 2021).

Because this paper focuses on thin- and thick-disc formation, we have refrained from presenting results on early *in situ* spheroid formation, though this would be an interesting topic for future work. It is worth noting that, when weighted by luminosity, the spheroidal components contribute minimally to the total light in our galaxies at  $z = 0$ .

### 3.1.3 Kinematic classification with time

Fig. 5 shows mass-weighted circularity distributions for star particles in *Romeo* (left) and *Juliet* (right). The black solid lines indicate distributions for *all* stars within  $R_{90}$  of each galaxy at  $z = 0$ . The blue lines indicate the  $z = 0$  circularities for stars that formed during

the early, bursty phase ( $t_{\text{birth}} < t_B$ ), whilst the red lines refer to those formed during the later steady phase. Stars that formed during the steady phase are much more circular (thin-disc like) in each case, peaking close to  $\epsilon = 1$ . The stars that formed during the early bursty phase show much less coherence in angular momentum, with high- $\epsilon$  peaks closer to  $\epsilon \sim 0.8$ , indicative of thick-disc kinematics. Note that the distributions are normalized such that the sum of the red and blue lines equals the black lines.

The grey curves in Fig. 5 show the  $\epsilon$  distributions for all stars in the main progenitor of each galaxy at two different lookback times: 8.4 Gyr ago (grey solid) and 4.7 Gyr ago (grey dashed). These are the same times visualized in the lower left and lower middle panels of Figs 3 and 4. *Romeo*, which had just finished its bursty phase by 4.7 Gyr ago, had a fairly prominent peak at high circularity at that time. *Juliet*, which was still in its bursty phase at that time, had a less well-ordered angular momentum distribution. Both galaxies were systematically less well-ordered 8.4 Gyr ago than they were 4.7 Gyr ago. Whilst *Romeo* had a small peak near  $\epsilon \sim 0.8$ , more characteristic of a thick-disc component, *Juliet* had a distribution peaked near  $\epsilon = 0$ , as expected for a spheroidal system. These differences in angular momentum structure mirror the morphological differences between these two galaxies at the same times shown in Figs 3 and 4.

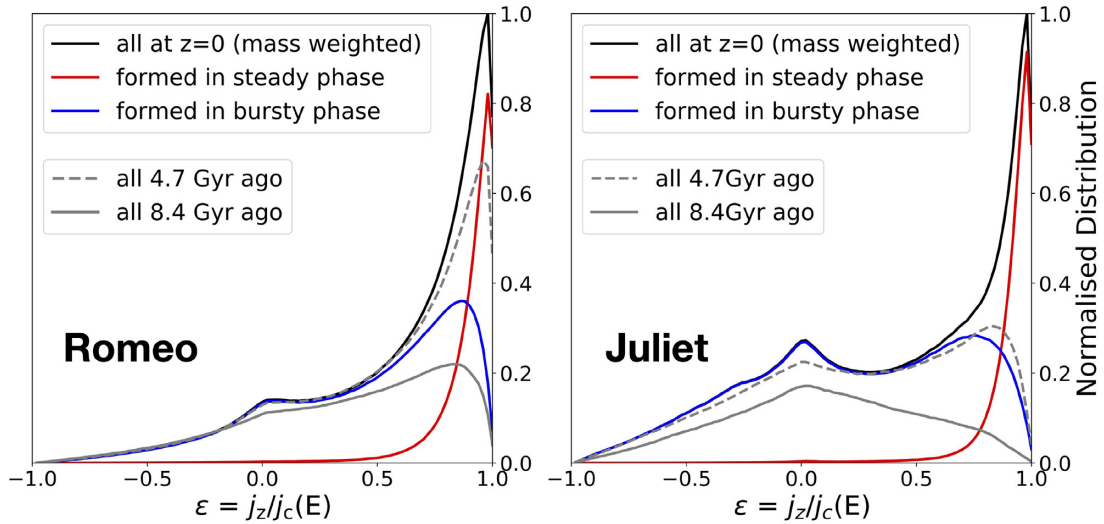


**Figure 5.** Circularity distributions for stars in *Romeo* (left) and *Juliet* (right). The solid black lines in each case show the mass-weighted distribution of stellar circularities ( $\epsilon$ ) for all stars within  $R_{90}$  of each galaxy (13.3 and 9.6 kpc, respectively) at  $z = 0$ . The solid red and blue lines correspond to stars formed in the steady star formation phase and the bursty phase, respectively. In each galaxy, stars that formed during the steady phase have high circularities, peaked near  $\epsilon = 1$ . Stars formed during the bursty phase are much less ordered, with a coherent rotation peak at  $\epsilon \lesssim 0.8$ , indicative of thick-disc kinematics. The grey solid and dashed lines show *total* mass-weighted star-particle distributions for the main progenitors of each galaxy 8.4 and 4.7 Gyr ago, respectively. *Romeo* (left), which ended its bursty phase 6.5 Gyr ago, had already developed a fairly substantial high-angular momentum peak 4.7 Gyr ago (dashed line), whilst *Juliet* (right), which ended its bursty phase only 4.4 Gyr ago, had only a modest thick-disc like peak at the same time. Further back in time, 8.4 Gyr ago, *Romeo* was much less ordered than it is today, but still had a thick-disc-like peak in stellar circularity. *Juliet*, on the other hand, had mostly spheroid-like kinematics, with a circularity distribution centred on  $\epsilon \sim 0$ , at this time.

### 3.2 Late-time mergers and starbursts

Three of our 12 galaxies (m12b, m12c, and m12f) experience late-time mergers after the steady phase has commenced (see Appendix A for details). We define a merger to be an event that impacts the central galaxy ( $< 20$  kpc) with a satellite that had a total mass (baryons and dark matter) greater than  $5 \times 10^{10} M_{\odot}$  when it crossed the inner 50 kpc. We record this as the merger time. Additionally, seven of our other galaxies have mergers of comparable sizes during the bursty phase, but these mergers do not correlate with disc properties in significant ways (see Appendix A).

Fig. 6 illustrates the star formation histories (top panels), total mass (dark matter plus baryons within 50 and 20 kpc) evolution (middle panels), and disc component age distributions (bottom panels) associated with m12b (left) and m12f (right). The bottom panel splits the age distribution into thin (cyan) and thick (magenta) disc stars. m12b experiences a polar-orbit merger with a gas-rich, Large Magellanic Cloud (LMC)-size satellite ( $\sim 10^{9.5} M_{\odot}$  in baryons,  $\sim 10^{11} M_{\odot}$  in dark matter) that coalesces at the time of the late-burst marked. The more prominent late-burst in m12f is associated with a merger with a satellite of a similar mass, but this time on a prograde orbit.

These late-time mergers and associated bursts do not change broad correlations we find between bursty-phase lookback time and thin-disc fractions and *median* thick-disc ages. However, they do enhance the age distribution of the youngest thick-disc stars. The lower panels of Fig. 6 include examples of this effect, where the thick-disc age distributions are not as sharply truncated after the bursty phase as they are in Fig. 2. This seems mostly to arise from heating associated with the merger, but feedback from the burst could also contribute. Interestingly, the burst also coincides with a peak in the *thin-disc* stellar age distribution. Many of the stars that form in these bursts apparently retain thin-disc orbits. That gas-rich mergers can promote stellar-disc formation is a well-known phenomenon (Robertson et al.

2006; Lian et al. 2020a, b). Santistevan et al. (2021) use the same simulations we analyse here to show that existing metal-poor stars and low-metallicity gas deposited in LMC-size mergers can explain the existence of low-metallicity prograde stars in the Milky Way (Sestito et al. 2020).

One of our 12 galaxies (*The1ma*) experiences a late-time burst ( $\sim 1$  Gyr lookback time) that is *not* associated with a merger. This appears to be a stochastic event associated with the fact that *The1ma* has only recently settled down to  $\sigma_{10}/\text{SFR}_{500} < 0.2$  at  $t_B = 2.6$  Gyr. Unlike the majority of our galaxies, *The1ma* does not settle down to a variance much smaller than 0.2; so the ‘burst’ by our formal definition looks more like a stochastic event. Only one other galaxy in our sample, m12w, never really settles down ( $t_B = 0.0$  Gyr) – its variance in instantaneous SFR around  $z = 0$  is still  $\sim 0.3$ .

### 3.3 Sample-wide trends

#### 3.3.1 Thick-disc age

Using four illustrative examples, Figs 2 and 6 suggest that the ages of kinematically identified thick-disc stars at  $z = 0$  tend to track the period of bursty star formation in these galaxies. The left-hand panel of Fig. 7 demonstrates that these trends hold for our entire sample. Displayed is the median age of thick-disc stars ( $t_{50}$ ) versus the bursty-phase lookback time ( $t_B$ ) for each galaxy. The correlation is quite tight, with more recent bursty phases associated with younger thick-disc ages. Note that  $t_B$  along the horizontal axis is determined entirely from the star formation history of the galaxy and includes no dynamical information whatsoever, and thus the observed correlation is non-trivial. For example, if thick discs were formed primarily from initially thin discs that were heated by mergers, we would expect no such correlation.



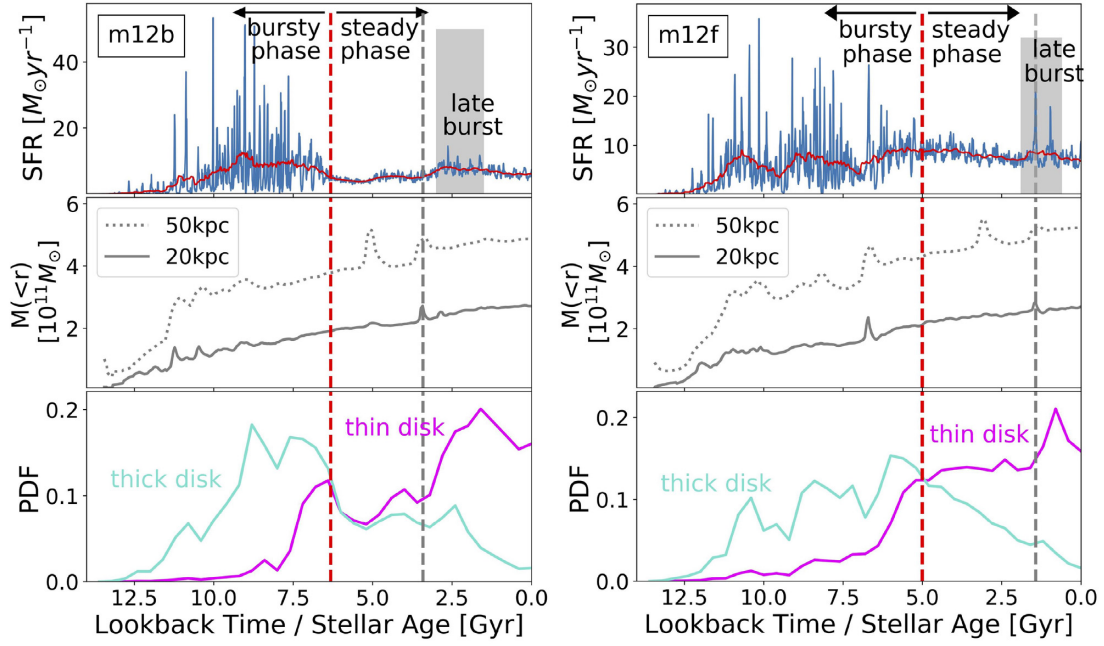


**Figure 6.** Star formation histories, mass assembly histories, and thin/thick-disc stellar age distributions for m12b (left) and m12f (right). These are examples of galaxies with late-time bursts triggered by minor mergers (shaded grey bars). The *top panels* show the SFR in each galaxy as a function of lookback time. The blue lines show the ‘instantaneous’ star formation rate averaged over 10 Myr bins, while the red lines show the ‘smoothed’ SFR averaged over 500 Myr bins. There are two distinct phases in the star formation history for each galaxy, an early bursty phase and a late steady phase. We divide the two at a time  $t_B$ , which we define as the time when the variance in instantaneous SFR falls below 0.2 times the smoothed SFR. This ‘bursty-phase lookback time’ is marked by the vertical red dashed line in each upper panel. The grey bands indicate late-time bursts of star formation that occur during the steady phase. The *middle panels* show the total mass of central galaxies within 50 kpc (grey dotted) and 20 kpc (grey solid), respectively, as a function of lookback time. From the mass assembly history, we see that the fairly significant burst in m12f was triggered by a late-time, prograde, LMC-size merger. The smaller burst in m12b was also triggered by the final coalescence of a merger, of similar size, but this time on a polar orbit.<sup>3</sup> We record the first central impact time of this type of mergers and mark with grey dashed lines in the plot. The *bottom panels* show the age distribution of  $z = 0$  stars that belong to the thick disc (cyan) and thin disc (magenta) in each galaxy. We see that thick-disc stars have ages that track closely the bursty period of star formation while thin-disc stellar ages correspond more closely to the steady phase. Stars made in the late-time bursts appear to populate the thin disc primarily, but some stars end up in the thick disc as well. The burst age is preceded by an enhanced tail of slightly older thick-disc stars, which is consistent with what would be expected from disc heating. These events do not change appreciably the median age of thick-disc stars but do enhance the post-steady-phase tail of the thick-disc stellar age distributions compared to cases without late bursts (compare to Fig. 2).

The typical (median) thick-disc star was formed approximately 3 Gyr prior to the end of the bursty phase. The red-dashed line shows the best-fitting linear relation:

$$t_{50} = 3.7 + 0.69t_B, \quad (2)$$

where times are assumed to be in units of Gyr. The Pearson correlation coefficient for the points in the left-hand panel is  $r = 0.89$  with  $p\text{-value} = 9.0 \times 10^{-5}$ . Although not shown, we find that the average age of thick-disc stars produces a very similar trend with bursty-phase lookback time as the median age displayed here. Given that the thick-disc population is primarily born during the bursty phase, it is natural to ask if the youngest thick-disc stars allow us to age-date the end of the bursty phase in a one-to-one way. We find that this is true only for the 9 of our 12 galaxies that *do not* have a late-time merger during the steady phase.

The right-hand panel of Fig. 7 shows the age of the ninetieth percentile youngest thick-disc star ( $t_{90}$ ) versus the bursty-phase lookback time (solid points). The dotted grey line shows the one-to-one relation for reference. The grey symbols refer to galaxies with late-time mergers, which clearly deviate from the trend. The one galaxy in our sample that experiences a late-time burst not triggered by a merger (The1ma, coloured pentagon) does not deviate significantly. The open grey symbols use the lookback time to the

late-time merger as the horizontal coordinate. With this choice, the points fall along a fairly tight relation (with Pearson correlation coefficient of  $r = 0.91$  and  $p\text{-value} = 3.0 \times 10^{-5}$ ). The dashed red line shows a linear fit to the coloured and open points (with solid grey points ignored):

$$t_{90} = 1.2 + 0.65t_B, \quad (3)$$

where times are assumed to be in units of Gyr.

The grey points in the left-hand panel of Fig. 7 represent galaxies with late-time mergers. This group tends to track the relation, but also tend to lie systematically below the average trend with respect to median age. This is consistent with the interpretation that the young-star tail of the thick-disc population has been populated by stars formed after the end of the bursty phase. Nevertheless, the fraction of stars populated in this way is small enough ( $\lesssim 10$  per cent) that the broad trend with median age and bursty phase lookback time is preserved.

Given that the youngest thick-disc stars may be associated with either the end of the bursty phase or a late-time merger, it may be difficult to use the age of the youngest stars to easily date the end of the bursty phase. In principle, one could look for features in the age distribution of thick-disc stars to gain insight on these questions (see Fig. 6 where the bursty lookback time does seem to imprint a feature

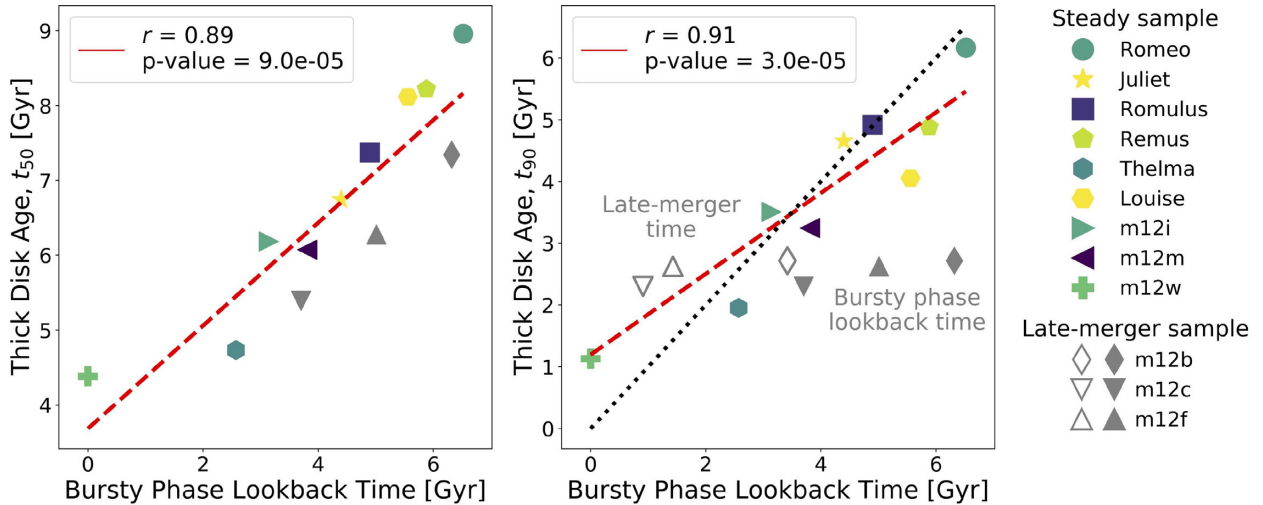


**Figure 7.** Correlation between the bursty-phase lookback time and thick-disc age for our entire sample. The grey points correspond to galaxies that experience late-time minor mergers after the steady phase has begun. *Left:* Median thick-disc age ( $t_{50}$ ) versus the lookback time to the end of the bursty phase. The legend (far right) displays a unique symbol type per galaxy. The dashed-red line shows a linear fit to the relation. The Pearson correlation coefficient ( $r = 0.89$ ) is boxed in the upper left. The typical age of a thick-disc star correlates quite strongly with the end of the bursty phase. *Right:* Age of ninetieth percentile youngest thick-disc star ( $t_{90}$ ) versus the lookback time to the end of the bursty phase (solid points). The solid grey points – those with late-time mergers – clearly lie on a different relation than the coloured points, suggesting that the late bursts influence and populate the young-star tail of the thick-disc population. The open points are the same galaxies, now depicted at the lookback time when the late-time merger occurred. These seem to align fairly closely to a one-to-one line (grey dotted), along with the coloured points. The red dashed line shows a linear fit to the open grey and coloured points.

in the age distribution of thick-disc stars). However, it will likely be more straightforward to use the typical age (median or average) of thick-disc stars to estimate the lookback time corresponding to the end of the bursty phase and the beginning of the steady phase (independent of the recent merger activities).

### 3.3.2 Thin-disc fraction

Fig. 8 shows the correlation between bursty-phase lookback time and thin-disc fraction, with each symbol type mapped to a specific galaxy name (far-right legend). The left-hand panel employs a mass-weighted thin-disc fraction, whilst the right-hand panel uses as luminosity-weighted thin-disc fraction. The red lines show linear fits to the data points. In each case, the correlation is strong, but with scatter, with Pearson correlation coefficients of  $r = 0.86$  (mass weighted) and  $r = 0.88$  (luminosity weighted). Both  $p$ -values ( $3.9 \times 10^{-4}$  and  $1.6 \times 10^{-4}$ , respectively) are much less than the significance level.

We see that the earlier the lookback time to the transition, the more prominent the thin disc is. It makes qualitative sense that the longer stars are created in the ‘settled’ phase, the larger the fraction of thin-disc stars we would see. At fixed thin-disc fraction, we see 2–3 Gyr scatter in the lookback time to the bursty phase. It would be surprising, however, if this relation were any tighter, as it contains no information on the absolute SFRs in either phase. Specifically, at fixed lookback time to the transition, the higher the average SFR during the thin-disc/steady phase compared to the thick-disc/bursty phase, the more prominent the thin disc would be. We see that this trend generally holds for our galaxies. For example, if we examine the star formation histories in Fig. 6 for galaxies m12b and m12f, we see that m12b has a higher smoothed-average SFR during the bursty phase than it does during the steady phase. Conversely, m12f has a similar smoothed-average SFR before and after the transition. This means that m12b will be making fewer thin-disc stars per unit

time during the steady phase than m12f. This explains why m12b has a thin-disc fraction (0.64 in luminosity) that is slightly lower than m12f (0.65), even though its steady phase lasts more than one billion years longer (7.34 Gyr versus 6.28 Gyr).

### 3.3.3 CGM virialization and steady star formation

The physical origin of the progression from early, bursty and less kinematically ordered star formation to late-time, steady star formation in thin discs is not clear. An important clue comes from the work of Stern et al. (2020), who used FIRE-2 simulations to show that the bursty to steady transition in galaxy star formation coincides with virialization of the inner CGM. They quantify inner CGM virialization using the ratio of the cooling time of shocked gas  $t_{\text{cool}}^{(s)}$  to the free-fall time  $t_{\text{ff}}$  at an inner radius  $r = 0.1R_{\text{vir}}$ . When  $t_{\text{cool}}^{(s)}/t_{\text{ff}} \gtrsim 1$  the inner CGM is smooth and largely supported by thermal pressure. In contrast, when  $t_{\text{cool}}^{(s)}/t_{\text{ff}} \lesssim 1$ , the inner CGM has large pressure fluctuations and is highly dynamic. Using a sample of sixteen zoom simulations with halo masses ranging from  $M_{\text{halo}} = 10^{10.6}$  to  $10^{13} M_{\odot}$ , Stern et al. (2020) shows that gaseous discs become rotationally supported and star formation transitions from bursty to steady at roughly the time when the ratio first becomes  $t_{\text{cool}}^{(s)}/t_{\text{ff}} > 2$ . Their sample included four of the 12 galaxies we consider here.

In this brief section, we extend the Stern et al. (2020) analysis to the additional haloes in our sample and confirm their reported trends. Using the same definitions of free-fall time and cooling time described in Section 2.1 of their paper, we show that inner CGM virialization at the time when  $t_{\text{cool}}^{(s)}/t_{\text{ff}} = 2$  generally coincides with our bursty to steady SFR transition at  $\sigma_{10}/\text{SFR}_{500} = 0.2$  (equation 1). This is demonstrated in Fig. 9, where we show the evolution of the inner virialization parameter (right axis, orange line) and the burstiness parameter (left axis, blue line) as functions of lookback time for six example haloes. Not only do the transition time-scales coincide in each case, but the

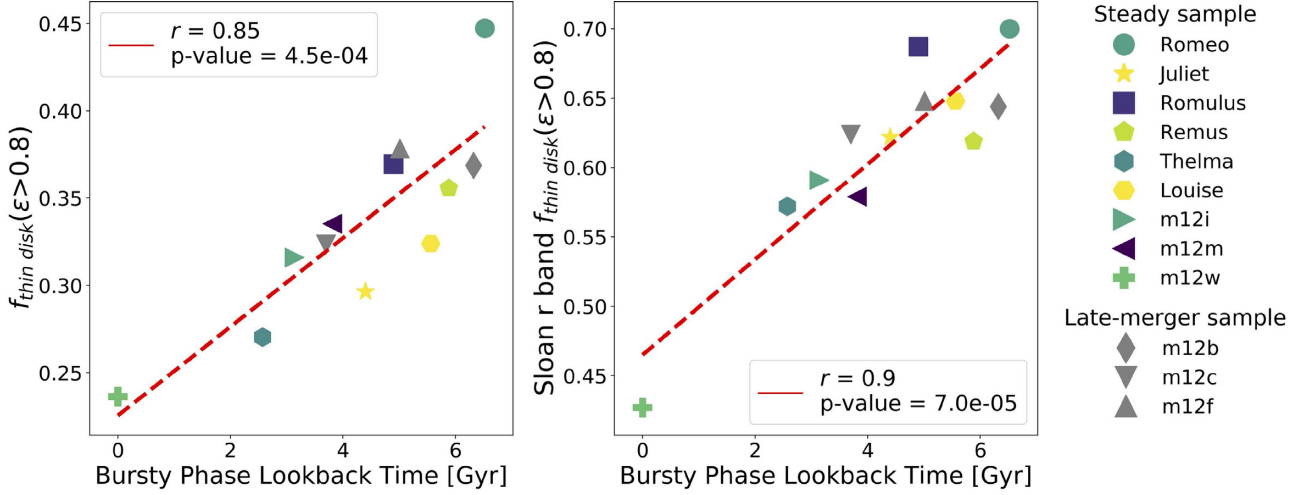


**Figure 8.** Correlations between the bursty-phase lookback time and the thin-disc fraction. *Left:* Mass-weighted thin-disc fraction versus bursty-phase lookback time for each run. The legend on the far-right relates each symbol to a unique galaxy in our sample, in the same manner as Fig. 7. *Right:* Luminosity-weighted thin-disc fraction versus bursty-phase lookback time. In both panels, galaxies with longer lookback times to the bursty phases (and hence the longer-lasting steady phases) have more pronounced thin disc. The red-dashed line in each panel shows a linear fit to the points. The corresponding Pearson correlation coefficient is listed. The correlation is significant ( $r > 0.8$ ) in each case, even though we have included no information on the relative average rate of star formation in the bursty (thick-disc) phase compared to the steady (thin-disc) phase. As in Fig. 7, we present the runs that have a recent minor merger in grey. There is no significant difference between these runs and the others in the thin-disc fraction at fixed bursty-phase lookback time.

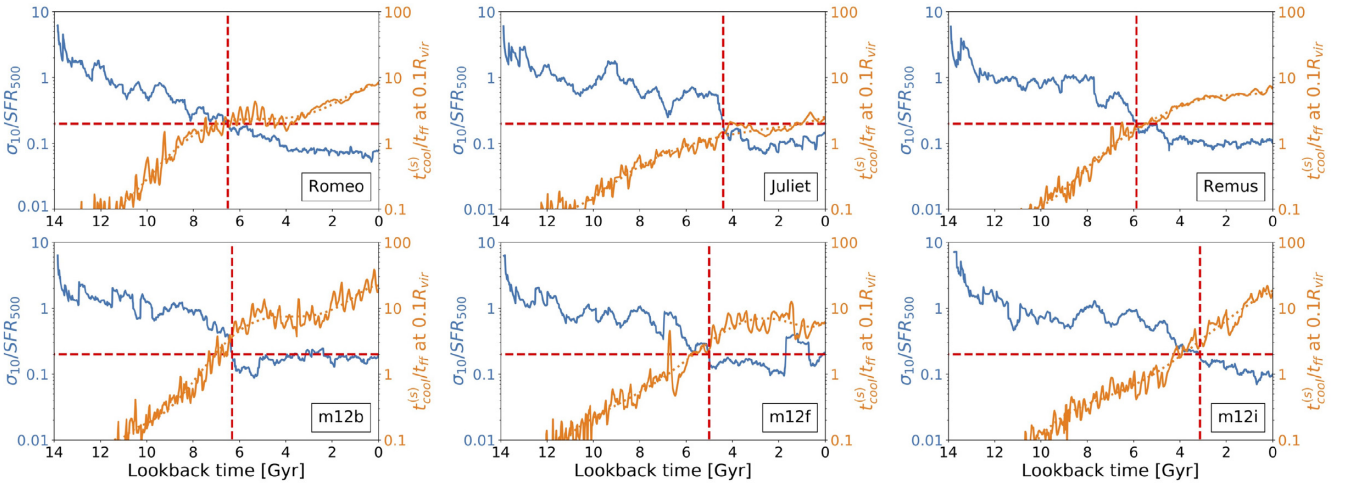


**Figure 9.** Parameters that track star formation burstiness (blue) and inner CGM virialization propensity (orange) as functions of lookback time for six of our haloes. As described in Section 3.3.3, the orange lines (right axis) show the cooling time to free-fall time ratio measured at  $0.1R_{\text{vir}}$  as a function of lookback time. The blue lines (left axis) shows the variance in instantaneous SFR divided by the smoothed SFR as a function of time. The horizontal red dashed line marks the threshold above which the inner CGM virialises,  $t_{\text{cool}}^{(s)}/t_{\text{ff}} \approx 2.0$ , as defined in Stern et al. (2020). The axes are set so that the same line corresponds to  $\sigma_{10}/\text{SFR}_{500} = 0.2$ , which we have adopted in this paper to define the end of the bursty phase. The bursty-phase lookback time  $t_B$  defined in this paper is marked by the vertical red dashed line. Note that the same time roughly corresponds to the time when the inner CGM becomes virialized.

monotonic progressions of each parameter tends to evolve inversely with the other in time. At early times, when gas flows are prone to cooling instabilities and clumpy accretion, the star formation is more bursty. At late times, when cooling times are long and the flow can be relatively smooth and well-mixed, star formation tends to be more constant. We find similar behaviours hold for every halo in our sample.

The proceeding analysis demonstrates that as the inner CGM of our galaxies virializes, the star formation becomes less bursty (Fig. 9).

This is also the time when stars tend to be formed with thin-disc kinematics (Fig. 7). One hypothesis that explains this, suggested by Stern et al. (2020), is that a virialized inner CGM enables the formation of stable discs because a hot and uniform halo can pressure-confine disruptive superbubbles driven by clustered supernovae. Another possibility is that smooth and well-mixed accretion enables more coherently aligned angular momentum at the time of accretion on to the galaxy (Hafen et al., in preparation). These issues are important topics for further exploration.



#### 4 DISCUSSION AND CONCLUSIONS

We investigate the formation of the stellar thin- and thick-disc components using 12 FIRE-2 zoom-in simulations of Milky Way-mass galaxies. Our main findings include the following:

- (i) Each galaxy experiences an early period of bursty star formation that transitions into a steady phase, with a relatively constant SFR at late times. The transition time corresponds to the time when the inner CGM becomes sub-sonic and virializes (Fig. 9).
- (ii) The transition from bursty to steady star formation correlates with a shift in the formation of stars with thick-disc kinematics to thin-disc kinematics (Figs 2–4).
- (iii) The lookback time to the end of bursty phase ranges from  $t_B = 0.0$  to 6.5 Gyr in our sample. This time correlates strongly with the median age of thick-disc stars at  $z = 0$  (Fig. 7).
- (iv) Galaxies with longer steady phases (larger  $t_B$ ) tend to have higher thin-disc fractions (Fig. 8).

Three of our 12 simulations have appreciable late-time mergers that occur after the steady (thin-disc) phase has commenced. These mergers are not responsible for the bulk of thick-disc stars, though they do heat some disc stars and populate the young-star tail of the thick-disc population demonstrated in Fig. 6 and the right-hand panel of Fig. 7.

The fact that our discs emerge thick and become thinner over cosmic time is consistent with previous findings of ‘upside-down’ disc formation (Brook et al. 2004, 2012; Bird et al. 2013; Ma et al. 2017b; Navarro et al. 2018; Park et al. 2020; Bird et al. 2021). However, our result that the transition is associated with a transition in star formation activity – from bursty to steady – adds a new element to this discussion. That FIRE simulations of Milky Way-mass haloes experience such a transition in star formation activity is not a new result (Muratov et al. 2015; Anglés-Alcázar et al. 2017b; Sparre et al. 2017; Faucher-Giguère 2018). The onset of the steady phase appears to be related to the virialization of the inner CGM (Stern et al. 2020, and Fig. 9). A hot, pressurized CGM may stabilise the disc against supernovae-driven outflows and enable thin-disc formation (Stern et al. 2020). If correct, this interpretation opens the possibility of using stellar archaeology to learn about the origin of the Milky Way’s CGM and its associated history of star formation modes.

Whilst a more observationally oriented comparison is required to interpret our results for the Milky Way confidently, it is tempting to explore some potential implications based on naïve comparisons to published estimates of the Galactic thick-disc age distribution (Haywood et al. 2013; Snaith et al. 2014; Martig et al. 2016; Hayden et al. 2017; Sharma et al. 2019). Most estimates suggest that the Milky Way thick-disc has a median age of  $\sim 9$  Gyr, with few stars younger than 6 Gyr. Such an age distribution is most similar to our *Romeo* simulation (Fig. 2), which transitioned from bursty to steady star formation  $\sim 6.5$  Gyr ago. This simple comparison would suggest that the Milky Way transitioned at a similar time, commensurate with the virialization of its inner hot halo. If this is the case, then prior to that time, the Milky Way lacked a dominant thin-disc component, was forming stars in a bursty manner, and had non-virialized inner CGM.

Related to our analysis, Bellardini et al. (2021), using the same set of simulations, finds that gas disc metallicity in-homogeneity was dominated by azimuthal variations at high redshift but then transitioned to being dominated by radial gradients at lower redshifts, which has also been reported in the previous analysis in the FIRE-1 simulations across a much wider galaxy mass range (Ma et al. 2017a). The transition epochs after which radial variations dominate

over azimuthal scatter agree broadly well with our measurement of the transitions from bursty to steady phase. Although there is significant scatter and some time delay between the measurements of two transition times, it shows some potential observable implications of the bursty/steady transition for galactic archaeology.

Some cosmological galaxy formation simulations, including those that demonstrate upside-down disc formation (e.g. Park et al. 2020), do not have early bursty star formation phases of the kind we witness in our models. This may partially be due to star formation threshold employed. Burstiness is suppressed in simulations with modest threshold densities ( $\sim 10 \text{ cm}^{-3}$ ) for star formation, whereas our simulations require  $\sim 1000 \text{ cm}^{-3}$  (see Benítez-Llambay et al. 2019; Dutton et al. 2019, for a related discussion). Given this, chemical tracers among the various Galactic kinematic components may provide a means to test star formation prescriptions. Other factors like the ISM model, local star formation efficiency and the stellar feedback model might also play a role. Future work in this direction will be illuminating.

#### ACKNOWLEDGEMENTS

SY and JSB were supported by NSF grants AST-1910346 and AST-1518291. CK was supported by a National Science Foundation Graduate Research Fellowship Program under grant DGE-1839285. JS is supported also by the German Science Foundation via DIP grant STE 1869/2-1 GE 625/17-1. AW received support from NASA through ATP grants 80NSSC18K1097 and 80NSSC20K0513; HST grants GO-14734, AR-15057, AR-15809, and GO-15902 from STScI; a Scialog Award from the Heising-Simons Foundation; and a Hellman Fellowship. Support for JM is provided by the NSF (AST Award Number 1516374). ZH was supported by a Gary A. McCue postdoctoral fellowship at UC Irvine. ABG was supported by an NSF-FGRFP under grant DGE-1842165 and was additionally supported by NSF grants DGE-0948017 and DGE-145000. Support for PFH was provided by NSF Research Grants 1911233 and 20009234, NSF CAREER grant 1455342, NASA grants 80NSSC18K0562, *HST*-AR-15800.001-A. Numerical calculations were run on the Caltech compute cluster ‘Wheeler,’ allocations FTA-Hopkins/AST20016 supported by the NSF and TACC, and NASA HEC SMD-16-7592. CAFG was supported by NSF through grants AST-1715216 and CAREER award AST-1652522; by NASA through grant 17-ATP17-0067; by STScI through grant *HST*-AR-16124.001-A; and by a Cottrell Scholar Award and a Scialog Award from the Research Corporation for Science Advancement. RF acknowledges financial support from the Swiss National Science Foundation (grant nos 157591 and 194814). We ran simulations using: XSEDE, supported by NSF grant ACI-1548562; Blue Waters, supported by the NSF; Pleiades, via the NASA HEC program through the NAS Division at Ames Research Center.

#### DATA AVAILABILITY

The data supporting the plots within this article are available on reasonable request to the corresponding author. A public version of the GIZMO code is available at <http://www.tapir.caltech.edu/~phopkins/Site/GIZMO.html>. Additional data including simulation snapshots, initial conditions, and derived data products are available at <https://fire.northwestern.edu/data/>. Some of the publicly available software packages used to analyse these data are available at [https://bitbucket.org/awetzel/gizmo\\_analysis](https://bitbucket.org/awetzel/gizmo_analysis) and <https://bitbucket.org/awetzel/utilities>.

## REFERENCES

- Abadi M. G., Navarro J. F., Steinmetz M., Eke V. R., 2003, *ApJ*, 597, 21
- Anglés-Alcázar D., Faucher-Giguère C.-A., Kereš D., Hopkins P. F., Quataert E., Murray N., 2017a, *MNRAS*, 470, 4698
- Anglés-Alcázar D., Faucher-Giguère C.-A., Quataert E., Hopkins P. F., Feldmann R., Torrey P., Wetzel A., Kereš D., 2017b, *MNRAS*, 472, L109
- Bellardini M. A., Wetzel A., Loebman S. R., Faucher-Giguère C.-A., Ma X., Feldmann R., 2021, preprint ([arXiv:2102.06220](https://arxiv.org/abs/2102.06220))
- Belokurov V., Erkal D., Evans N. W., Koposov S. E., Deason A. J., 2018, *MNRAS*, 478, 611
- Benítez-Llambay A., Frenk C. S., Ludlow A. D., Navarro J. F., 2019, *MNRAS*, 488, 2387
- Bensby T., Feltzing S., Lundström I., Ilyin I., 2005, *A&A*, 433, 185
- Bensby T., Alves-Brito A., Oey M. S., Yong D., Meléndez J., 2011, *ApJ*, 735, L46
- Bird J. C., Kazantzidis S., Weinberg D. H., Guedes J., Callegari S., Mayer L., Madau P., 2013, *ApJ*, 773, 43
- Bird J. C., Loebman S. R., Weinberg D. H., Brooks A. M., Quinn T. R., Christensen C. R., 2021, *MNRAS*, 503, 1815
- Bovy J., Rix H.-W., 2013, *ApJ*, 779, 115
- Bovy J., Rix H.-W., Hogg D. W., 2012, *ApJ*, 751, 131
- Brook C. B., Kawata D., Gibson B. K., Freeman K. C., 2004, *ApJ*, 612, 894
- Brook C. B., Kawata D., Martel H., Gibson B. K., Bailin J., 2006, *ApJ*, 639, 126
- Brook C. B. et al., 2012, *MNRAS*, 426, 690
- Dutton A. A., Macciò A. V., Buck T., Dixon K. L., Blank M., Obreja A., 2019, *MNRAS*, 486, 655
- Elmegreen B. G., Elmegreen D. M., 2006, *ApJ*, 650, 644
- Elmegreen D. M., Elmegreen B. G., Ravindranath S., Coe D. A., 2007, *ApJ*, 658, 763
- Elmegreen B. G., Elmegreen D. M., Tompkins B., Jenks L. G., 2017, *ApJ*, 847, 14
- Escala I. et al., 2018, *MNRAS*, 474, 2194
- Faucher-Giguère C.-A., 2018, *MNRAS*, 473, 3717
- Faucher-Giguère C.-A., Lidz A., Zaldarriaga M., Hernquist L., 2009, *ApJ*, 703, 1416
- Flores Velázquez J. A. et al., 2021, *MNRAS*, 501, 4812
- Freudenburg J. K. C., Weinberg D. H., Hayden M. R., Holtzman J. A., 2017, *ApJ*, 849, 17
- Fuhrmann K., 1998, *A&A*, 338, 161
- Garrison-Kimmel S., Boylan-Kolchin M., Bullock J. S., Lee K., 2014, *MNRAS*, 438, 2578
- Garrison-Kimmel S. et al., 2017, *MNRAS*, 471, 1709
- Garrison-Kimmel S. et al., 2019a, *MNRAS*, 487, 1380
- Garrison-Kimmel S. et al., 2019b, *MNRAS*, 489, 4574
- Genzel R. et al., 2008, *ApJ*, 687, 59
- Gilmore G., Reid N., 1983, *MNRAS*, 202, 1025
- Grand R. J. J. et al., 2018, *MNRAS*, 474, 3629
- Hayden M. R. et al., 2015, *ApJ*, 808, 132
- Hayden M. R., Recio-Blanco A., de Laverny P., Mikolaitis S., Worley C. C., 2017, *A&A*, 608, L1
- Haywood M., Di Matteo P., Lehnert M. D., Katz D., Gómez A., 2013, *A&A*, 560, A109
- Helmi A., Babusiaux C., Koppelman H. H., Massari D., Veljanoski J., Brown A. G. A., 2018, *Nature*, 563, 85
- Hopkins P. F., 2015, *MNRAS*, 450, 53
- Hopkins P. F., 2016, *MNRAS*, 455, 89
- Hopkins P. F., 2017, *MNRAS*, 466, 3387
- Hopkins P. F. et al., 2018, *MNRAS*, 480, 800
- Jurić M. et al., 2008, *ApJ*, 673, 864
- Kassin S. A. et al., 2012, *ApJ*, 758, 106
- Katz N., Weinberg D. H., Hernquist L., 1996, *ApJS*, 105, 19
- Kazantzidis S., Bullock J. S., Zentner A. R., Kravtsov A. V., Moustakas L. A., 2008, *ApJ*, 688, 254
- Knebe A. et al., 2013, *MNRAS*, 428, 2039
- Krumholz M. R., Gnedin N. Y., 2011, *ApJ*, 729, 36
- Lee Y. S. et al., 2011, *ApJ*, 738, 187
- Lehnert M. D., Di Matteo P., Haywood M., Snaith O. N., 2014, *ApJ*, 789, L30
- Lian J. et al., 2020a, *MNRAS*, 494, 2561
- Lian J. et al., 2020b, *MNRAS*, 497, 2371
- Ma X., Hopkins P. F., Feldmann R., Torrey P., Faucher-Giguère C.-A., Kereš D., 2017a, *MNRAS*, 466, 4780
- Ma X., Hopkins P. F., Wetzel A. R., Kirby E. N., Anglés-Alcázar D., Faucher-Giguère C.-A., Kereš D., Quataert E., 2017b, *MNRAS*, 467, 2430
- Mackereith J. T. et al., 2017, *MNRAS*, 471, 3057
- Martig M., Minchev I., Ness M., Fouesneau M., Rix H.-W., 2016, *ApJ*, 831, 139
- Martizzi D., 2020, *MNRAS*, 492, 79
- Meng X., Gnedin O. Y., 2021, *MNRAS*, 502, 1433
- Muratov A. L., Kereš D., Faucher-Giguère C.-A., Hopkins P. F., Quataert E., Murray N., 2015, *MNRAS*, 454, 2691
- Navarro J. F. et al., 2018, *MNRAS*, 476, 3648
- Nikakhtar F. et al., 2021, preprint ([arXiv:2104.08394](https://arxiv.org/abs/2104.08394))
- Okamoto T., Frenk C. S., Jenkins A., Theuns T., 2010, *MNRAS*, 406, 208
- Oñorbe J., Garrison-Kimmel S., Maller A. H., Bullock J. S., Rocha M., Hahn O., 2014, *MNRAS*, 437, 1894
- Orr M. E. et al., 2018, *MNRAS*, 478, 3653
- Overzier R. A., Heckman T. M., Schiminovich D., Basu-Zych A., Gonçalves T., Martin D. C., Rich R. M., 2010, *ApJ*, 710, 979
- Park M. J. et al., 2021, *ApJS*, 254, 2
- Pillepich A. et al., 2019, *MNRAS*, 490, 3196
- Prochaska J. X., Naumov S. O., Carney B. W., McWilliam A., Wolfe A. M., 2000, *AJ*, 120, 2513
- Purcell C. W., Kazantzidis S., Bullock J. S., 2009, *ApJ*, 694, L98
- Quinn P. J., Hernquist L., Fullagar D. P., 1993, *ApJ*, 403, 74
- Recio-Blanco A. et al., 2014, *A&A*, 567, A5
- Robertson B., Bullock J. S., Cox T. J., Di Matteo T., Hernquist L., Springel V., Yoshida N., 2006, *ApJ*, 645, 986
- Samuel J. et al., 2020, *MNRAS*, 491, 1471
- Sanderson R. E. et al., 2020, *ApJS*, 246, 6
- Santistevan I. B., Wetzel A., Sanderson R. E., El-Badry K., Samuel J., Faucher-Giguère C.-A., 2021, preprint ([arXiv:2102.03369](https://arxiv.org/abs/2102.03369))
- Sestito F. et al., 2020, *MNRAS*, 497, L7
- Shapiro K. L. et al., 2008, *ApJ*, 682, 231
- Sharma S. et al., 2019, *MNRAS*, 490, 5335
- Sharma S., Hayden M. R., Bland-Hawthorn J., 2020, preprint ([arXiv:2005.03646](https://arxiv.org/abs/2005.03646))
- Snaith O. N., Haywood M., Di Matteo P., Lehnert M. D., Combes F., Katz D., Gómez A., 2014, *ApJ*, 781, L31
- Sparre M., Hayward C. C., Feldmann R., Faucher-Giguère C.-A., Muratov A. L., Kereš D., Hopkins P. F., 2017, *MNRAS*, 466, 88
- Stern J. et al., 2020, preprint ([arXiv:2006.13976](https://arxiv.org/abs/2006.13976))
- Su K.-Y., Hopkins P. F., Hayward C. C., Faucher-Giguère C.-A., Kereš D., Ma X., Robles V. H., 2017, *MNRAS*, 471, 144
- van der Kruit P. C., Freeman K. C., 2011, *ARA&A*, 49, 301
- Weinberg D. H. et al., 2019, *ApJ*, 874, 102
- Wetzel A. R., Hopkins P. F., Kim J.-h., Faucher-Giguère C.-A., Kereš D., Quataert E., 2016, *ApJ*, 827, L23

## APPENDIX A: MERGER HISTORIES

As discussed in Section 3.2, we have explored the importance of mergers in shaping thin/thick-disc formation in our simulations. In particular, we focus on merging events that perturb the total mass content within 20 kpc by more than  $2 \times 10^{10} M_{\odot}$  in the final coalescence of a satellite and that the merging satellite crossed within the 50 kpc sphere for the first time with more than  $5 \times 10^{10} M_{\odot}$  of total mass (which includes both dark matter and baryons). We have made these choices because only above these thresholds do we discern any correlated activity that influences star formation or disc structure.

Fig. 6 showed the mass assembly histories (middle panels) for two galaxies that experience late-time mergers by this definition. These

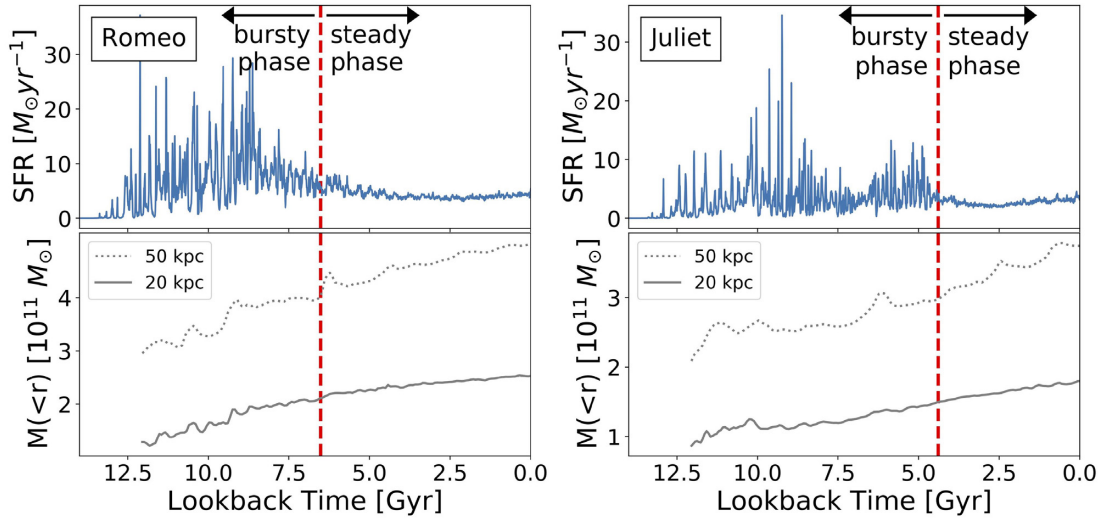


**Figure A1.** Star formation histories and mass assembly histories for Romeo (left) and Juliet (right). The solid and dotted lines in the lower panel show the total mass within 20 and 50 kpc of the main galaxy, respectively, as a function of time. We see that the mass growth is quite steady within 20 kpc, as expected for galaxies without significant merger activities.

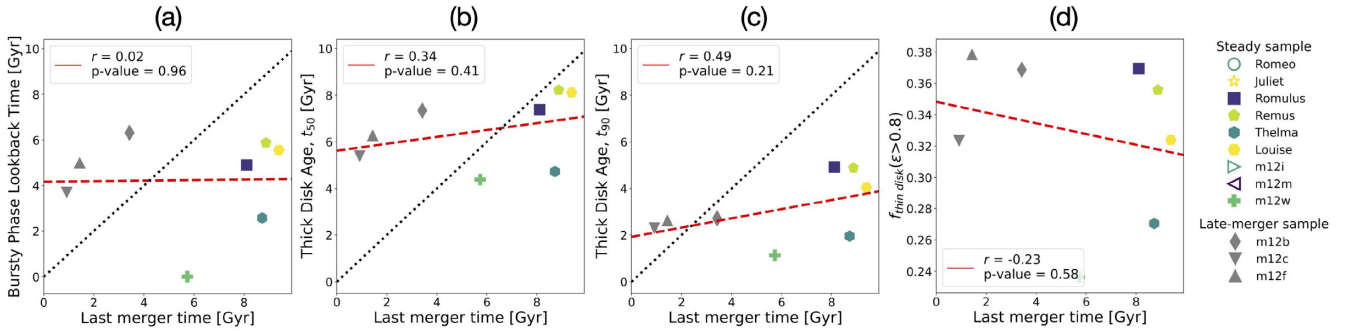


**Figure A2.** Correlations between the bursty-phase lookback time, thick-disc age, thin-disc fraction, and the last merger lookback time. (a) Bursty-phase lookback time versus the last merger lookback time for each run. We record the merger time as the first central impact time as indicated by the grey dashed line in the middle panel of Fig. 6. (b) Median thick-disc age ( $t_{50}$ ) versus the last merger lookback time. (c) Ninetieth percentile youngest thick-disc stars ( $t_{90}$ ) versus the last merger lookback time. (d) Mass-weighted thin-disc fraction versus the last merger lookback time. The legend (far right) shows the unique symbol type per galaxy similar to Figs 7 and 8. Note that, coloured open markers are not plotted and they correspond to the galaxies that we do not identify any recent mergers from the mass assembly histories. In all panels, we see no significant correlations.

mergers happened after the steady phase has commenced and appear to trigger late-time starbursts and also to add to the young-start tail of the age distribution of thick-disc stars. Fig. A2 shows example mass growth histories for two galaxies without such mergers. They also show star formation histories, specifically for Romeo (left) and Juliet (right). The lower panels show total mass within 50 kpc (dotted) and 20 kpc (solid) for each galaxy. We see that the central galaxies themselves experience little in the way of merger activity that perturbs their overall masses going back prior to the time the steady phase began (red dashed lines). Nevertheless the transition from bursty to steady phase is sharp, and these transition times correlate with thick-disc ages (Fig. 7) and thin-disc fractions (Fig. 8).

We have tabulated the lookback times of the last  $M_{\text{tot}} > \times 10^{10} M_{\odot}$  mergers in each of our simulated galaxies. Fig. A1 shows these times plotted against the bursty-phase lookback time, thick-disc age, and thin-disc fraction for our galaxies. Four galaxies, Romeo, Juliet, m12i, and m12m, experience no such merger over their lifetimes and are not plotted. We find no correlation between the last merger time and bursty-phase lookback time (left-hand panel). We find, at best, weak correlations with thick-disc age. A more detailed analysis of possible correlations between mergers and bursty/steady transition is deferred for future work.

This paper has been typeset from a  $\text{\LaTeX}$  file prepared by the author.